Modeling Pelvis Contact during Lateral Falls: Multi-Criteria Evaluation of Model Performance and Error Source Identification

I.C. Levine[1,2], S.P. Pretty[1], and A.C. Laing[1]

[1] Injury Biomechanics and Aging Laboratory, University of Waterloo, Waterloo, ON; [2] Home & Community Research Team, Toronto Rehabilitation Institute-UHN, Toronto, ON

ABSTRACT

Hip fractures are a substantive public health issue. Simple mass-spring or mass-spring-damper systems have been utilized to model lateral fall on the hip. However, the biofidelity of these models is questionable as the femur/pelvis system is comprised of complex interactions between biological soft and skeletal tissues. This study investigated how increasing the complexity of contact models (from geometric and damping perspectives) influenced the accuracy of impact dynamics predictions during sideways falls, and the biomechanical sources of errors for each model. Forty-six participants (<35 years) underwent simulated sideways falls which involved their pelvis impacting a force plate with a low (but clinically relevant) velocity of 1 m/s. Simulations implementing five contact models (mass-spring(MS), Voigt(VG), Hertzian (HZ), Hunt-Crossley(HC), and volumetric(VO)) estimated normal force during impact. Subject-specific input parameters (mass, stiffness, and damping) were incorporated using previously- derived regression equations. Model predictions were evaluated against subject-specific experimental data to determine five error metrics including: peak force magnitude (Err_{max}), loading duration (Err_{TTP}), RMSE error over the impact period (Err_{RMSE}), impulse (Err_{imp}), and prediction within an experimental corridor (Err_{corr})). Peak force estimates were substantively over-predictive for MS and VO, substantively under-predictive for VG, and best for HZ and HC. Time- to- peak force and impulse predictions were best for models with damping components (i.e. VG and HC, VO) but significantly over-predictive for MS and HZ. Err_{corr} and Err_{RMSE} were substantially improved for HC compared to all other models. Model errors were primarily linked to body composition, particularly body fat, overall body size, and floor-pelvis contact profile. Overall model performance was best for HC compared to all other models. Future model iterations should focus on characterizing the influence of body fat and adjusting contact geometry assumptions approximate shape and size of the floor-pelvis contact profile.

INTRODUCTION

Fall-related injuries form up to 85% of injury-related hospitalizations in adults over the age of 65, 40-60% which are hip fractures (Stinchcombe, 2014). A potential strategy to predict fall-related injury risk is a multibody systems approach, which allows rapid estimation of loading magnitude and distribution across several body regions simultaneously. However, it is unknown how model complexity might affect predictive capability, or provide better understanding of interactions between the pelvis and compliant protective devices such as safety floors (Laing, 2006) and hip protectors (Robinovitch, 2009).

Within this approach, impacts to the hip have typically been modeled as a simple single-degree-of-freedom (SDF) model, consisting of a mass, spring, and damper following Hooke's law (Laing, 2010; Robinovitch, 1991, Robinovitch, 1997a, Figure 1). This approach assumes soft tissues overlying the hip act in a two-dimensional energy absorption mechanism. SDF models with linear stiffness and damping parameters are associated with underprediction of time to peak force across velocity conditions, underprediction of peak force at high impact velocity and overprediction of peak force at low impact velocity (Robinovitch, 1997b), and produce inaccurate force predictions at body mass index (BMI) beyond 22.5-28 kg/m^2 (Levine, 2013). To counteract these errors and mimic the initial non-linear rise of force at impact, Laing et al. (2010) implemented non-linear stiffness estimates, matching the initial rise of force more closely; however these parameters were not explicitly linked to standard Hookean models nor individual characteristics such as body composition. Additionally, model performance evaluation focused solely on a single criterion, peak force prediction error; performance in recreating timing characteristics is unknown. While simple to parameterize, and rapid to implement, errors in existing models reveal that a one-dimensional approach may be too drastic a simplification.

Conversely, models based on Hertz contact theory, and Volumetric models incorporating three-dimensional geometry of the interacting bodies (i.e. the pelvis system and floor), may better represent the non-linear loading response of the pelvis during impact, and link this response to the spatial distribution of loading associated with soft tissues overlying the hip. In addition to improved peak force prediction, complex models may provide better understanding of interactions between the pelvis and compliant protective devices such as safety floors (Laing, 2006) and hip protectors (Robinovitch, 2009). The Hertz model, and the derivative Hunt-Crossley model (Hunt, 1975) employ non-linear spring and damping components, both with exponents of $^3/_2$, reflecting sphere-on-plane contact. To simulate non-linear generation of deformation and stress, stiffness and damping parameters for Volumetric contact models are governed by time-varying geometry of the interaction between the bodies. However, it is untested whether inclusion of geometric parameters improve loading characteristic prediction during an impact to the hip. Additionally, deviation of the pelvis-floor system from the sphere-on-plane contact assumption may negatively affect the accuracy of these models—this has not yet been tested.
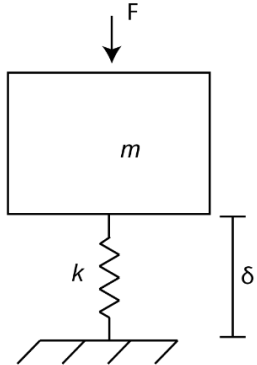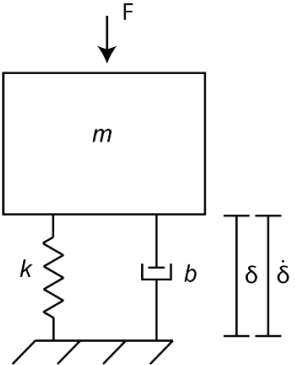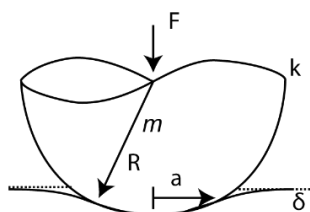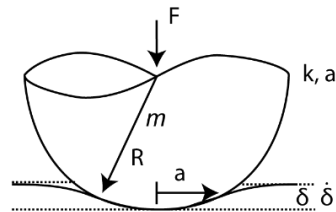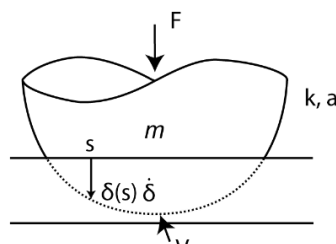
	Damping	
	No	Yes

Load Distribution

Point

F m k δ

Mass-Spring

$$F_N = k_{MS}\delta$$

F m k b δ $\dot{\delta}$

Voigt

$$F_N = k_{VG}\delta + b_{VG}\dot{\delta}$$

Geometric, point

F k m R a δ

Hertzian

$$F_N = k_{HZ}\delta^{3/2}$$

F k, a m R a δ $\dot{\delta}$

Hunt-Crossley

$$F_N = k_{HC}\delta^{3/2} + a_{HC}\delta^{3/2}\dot{\delta}$$

Geometric, distributed

F k, a m s $\delta(s)$ $\dot{\delta}$ V

Volumetric

$$F_N = k_{VO}V(1+a_{VO}\dot{\delta})$$

Figure 1: Model Schematics and normal force formulae for MS, VG, HZ, HC and VO. k refers to the stiffness coefficient for each model. b is the damping coefficient for single-degree-of-freedom models, while a is the damping coefficient for geometric models. Each of these constants is model-specific, and determined based on individual body size and composition. δ is the deflection, or depth of interaction, between the pelvis and floor, and is determined computationally during the modeling process.

Damped Hookean and Hertzian systems may further improve model biofidelity. In static scenarios, both the mass-spring and Hertz models have successfully modeled biological systems (Fregly, 2003; Gefen, 2007). However, biological systems behave viscoelastically due to fluid within the tissues exhibiting velocity-dependent resistance to deformation, energy dissipation, and decreases post-impact force oscillation. The performance improvement derived from interaction of damping and geometric components has not yet been tested for fall-related impacts.

Therefore, the primary goal of this study was to determine improvement in model performance, across a robust set of criteria, from the addition and interaction of: a) damping, and b) geometric components. Voigt (VG), Hunt-Crossley (HC) and Volumetric (VO) models were used to investigate the effect of damping, while Hertzian (HZ) and HC models were used to explore the effect of geometric considerations. We hypothesized that geometry and damping would interact, with HC and VO performing substantially better than VG or HZ, and MS performing substantially worse. The second goal of this study was to identify links between current model performance errors and individual characteristics to improve parameterization for future model iterations. We anticipated Hookean model accuracy would be worse outside a BMI range of 22.5-28, and that models would be particularly sensitive to body mass, and body fat percentage (BF). The final goal was to determine whether deviations from a circular contact profile (Levine, 2017) influenced geometric model performance.

METHODS

Forty-six healthy participants (<35 years, 24 female) consented to participate (Table 1). Exclusion criteria included health conditions which would make participation unsafe or prevent completion of the protocol. Participant mass (*mass*) was recorded to 0.5 kg. Hip circumference ($Circ_{hip}$) was measured with a flexible tape measure at the level of the greater trochanter, and height (*height*) and pelvis width (from right to left anterior superior iliac spine, *PW*) with a rigid meter stick, to 0.5 cm. Skinfold calipers were used to estimate *BF* via a seven-site method (Jackson, 1978; Jackson, 1979). Transverse-plane trochanteric soft tissue thickness (*TSTT*) was assessed via ultrasound (precision 0.17 cm; C60x, 2-5 MHz transducer, M-Turbo Ultrasound, SonoSite, Inc., Bothell, WA) in a side-lying position, similar to that expected during the impact phase of the fall simulations.

Table 1: Mean (SD) participant anthropometric characteristics. TSTT represents trochanteric soft tissue thickness. BMI represents body mass index

	Females (N = 24)				Males (N = 22)			
	Mean	SD	Max	Min	Mean	SD	Max	Min
Height (m)	1.65	0.06	1.72	1.52	1.79	0.07	1.94	1.69
Mass (kg)	68.6	18.9	130.0	47.0	81.6	11.6	107.0	55.0
BMI (kg/m^2)	25.1	6.8	45.5	17.9	25.4	3.3	30.4	18.6
TSTT (cm)	4.6	2.0	10.2	2.5	3.5	1.4	7.0	1.5
Pelvis Width (cm)	27.3	4.1	35.0	18.0	27.2	3.5	31.0	18.0
Hip Circumference (cm)	103.3	13.5	133.0	88.0	103.4	6.4	115.0	88.0
Body Fat (%)	36.4	13.6	61.4	16.2	22.1	9.1	43.0	8.0

Experimental protocol

Participants underwent a three-trial pelvis release protocol. The pelvis of the participant was supported by the sling (Figure 2), designed to not directly contact tissues between the iliac crest (superior border) and mid-thigh (inferior border). The upper body of the participant was supported by a pillow, while the feet rested on a mat, both outside the contact area of the force plate. The hips of the participant were flexed to 45° and knees were flexed to 90°. The sling was raised so that the soft tissues over the left hip were 5 cm above the impact surface. When the participant reported that they were "relaxed and ready", the electromagnet was released, allowing the lateral aspect of the left hip to impact a force plate (500 Hz; OR6-7, AMTI, USA) overlying a pressure plate (500 Hz; FootScan, RSScan, Olen, Belgium).
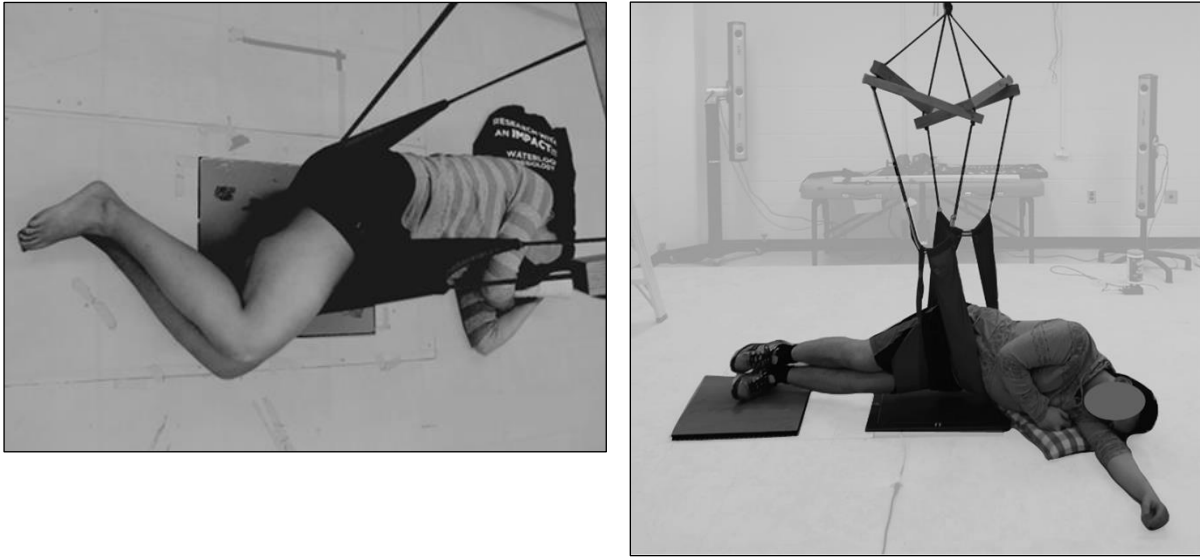

Figure 2: Initial position of the participant during the pelvis release protocol. The pelvis of the participant was suspended in a sling, supported by a set of ropes connected to a turnbuckle and an electromagnet. The electromagnet was release to allow the sling to release rapidly and allow the pelvis of the participant to impact the force plate.

Signal Processing

We processed time-varying signals with a customized MATLAB routine (MathWorks, Natick, MA. An automated point-selection routine segmented data: preceding unloaded region ($F_{initial}$), impact initiation (force exceeding two standard deviations of the mean within $F_{initial}$: T_{imp}, F_{imp}), peak force (T_{max}, F_{max}), and first minimum of force following F_{max} (T_{min}, F_{min}). Bias ($F_{initial}$) was subtracted from all force values. Time to peak (*TTP*) was estimated between T_{imp} and T_{max}. Impulse was calculated between T_{imp} and T_{min} as:

$$I = \int_{T_{imp}}^{T_{min}} F_t dt \qquad (1)$$

A force corridor (two standard deviations, Figure 3, grey band) for model validation was established based on experimental data between T_{imp} and T_{min}.
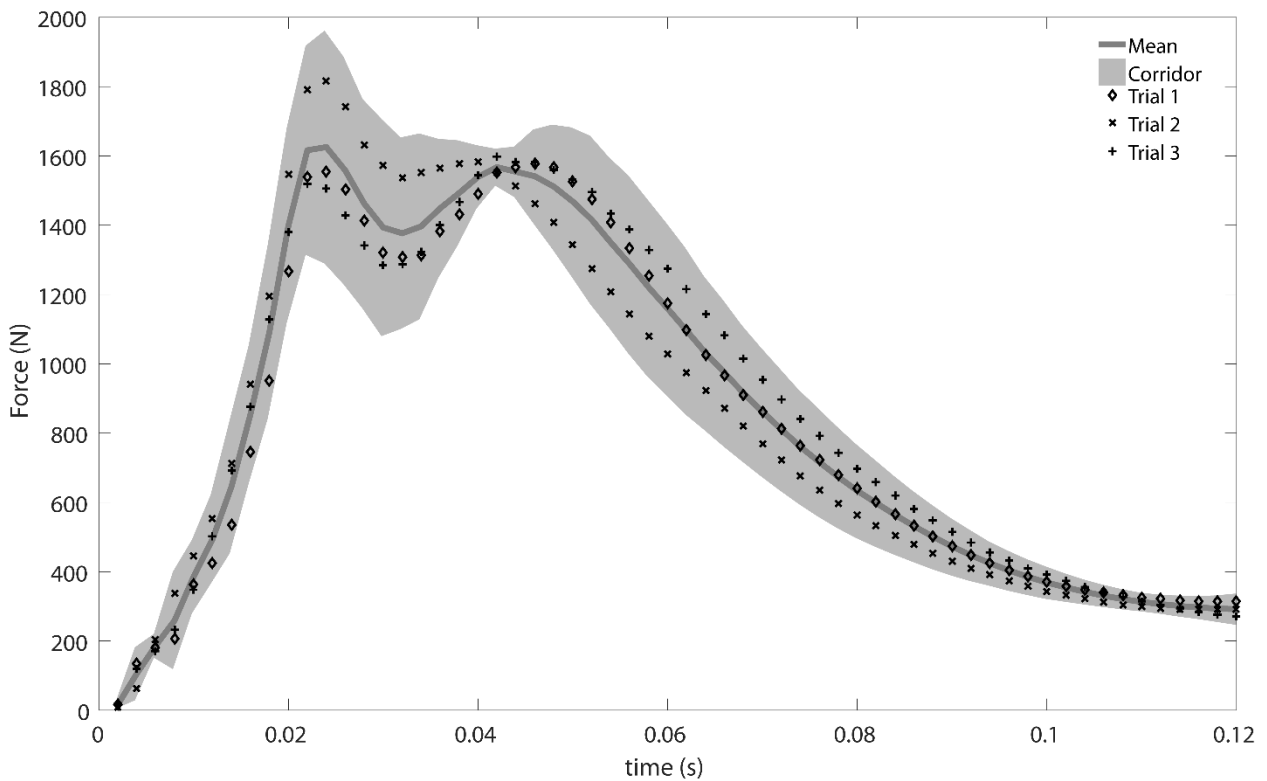

Figure 3: Experimentally-determined loading response corridors. Trial data were used to develop a time-varying mean (grey line) and two-standard-deviation corridor (grey band) for comparison.

Contact profile was determined using Radial Fourier Analysis (Ehrlich, 1970), the process for which, in this context, has been described previously (Levine, 2017a, Figure 4). Briefly, the polar coordinates of the shape of the pelvis-floor contact plane are analyzed to determine the primary constructive elements. H0 was interpreted as a metric of total contact area, H1 as circularity, and H2 as ellipticality of the contact profile.
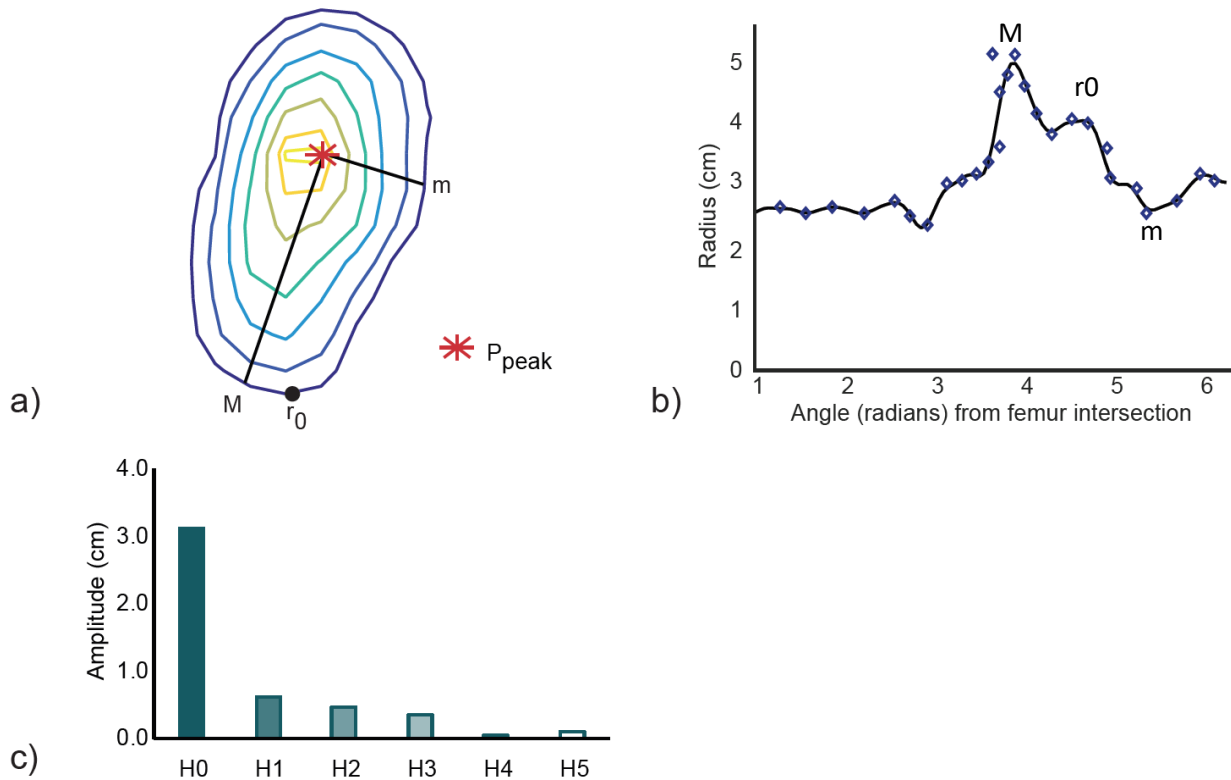
Figure 4: Analysis of the floor-pelvis contact profile. The perimeter of the contact area (indigo line, a) is used to develop a waveform (b). Radii are determined. Femur intersection point (r0), major axis (M) and minor axis (m) are demonstrated in panes a and b. The waveform is analyzed to produce harmonic amplitudes (c).

Characterization of impact dynamics and definition of model parameters

Parameter characterization is discussed in greater detail in a linked study (Levine, 2017b). Briefly, deflection and contact area of the pelvis were quantified during the impact phase of the experimental protocol using a different initial height (2 cm vs. 5 cm), two impact conditions (dynamic freefall, and quasi-static manual lowering at <2mm/min), and a subset of participants (14 males, 17 females). The resulting loading-phase force, deflection and volume data curves were fit using a least-squares approach to characterize stiffness and damping parameters (Figure 5). Experimental parameters were then linked to individual body geometry and composition characteristics (Table 2), and the regression models were used to estimate the parameters for this study.
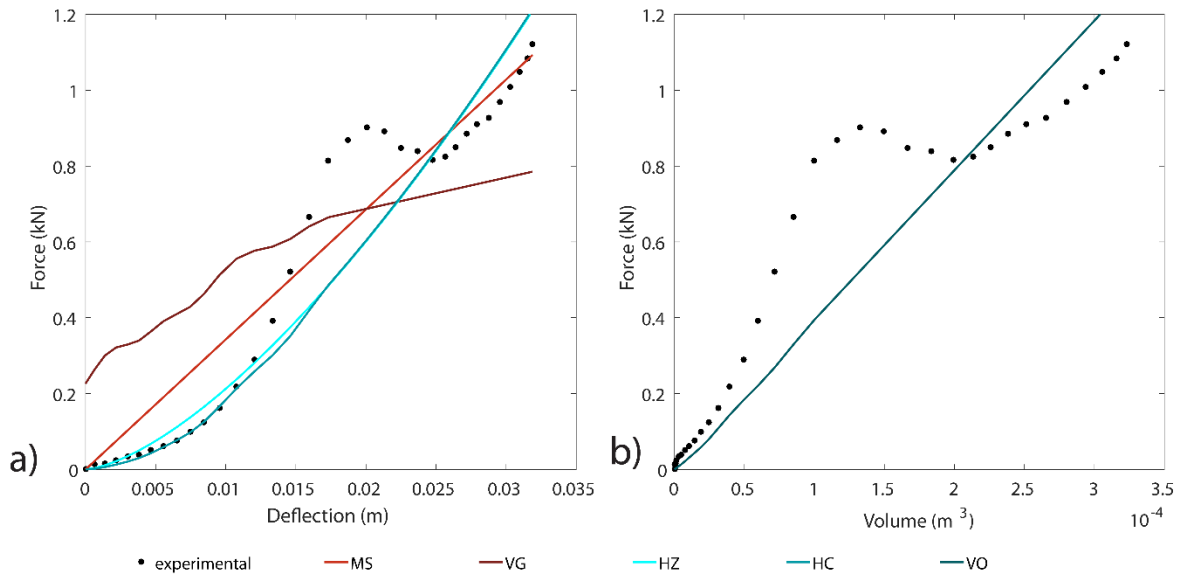
Figure 5: Demonstration of curve fit to experimental data for: a) MS, HZ, VG, HC, and b) VO. The experimental data (dots) is shown along with the final curve fit for each model, comprised of mass and stiffness (MS, HZ) or combined mass, stiffness and damping (VG, HC, VO) components.

Table 2 Model parameters

Parameter			Males	Females
Effective Mass			$m_{total}/2$ kg	$m_{total}/2$ kg
Pelvis Diameter			$(Circ_{hip}/\pi)$ m	$(Circ_{hip}/\pi)$ m
k		MS	$(-304.8*BF)+42699.7$ N/m	$(-304.8*BF)+42699.7$ N/m
		HZ	$(-3452.7*BF)+326489.1$ $N/m^{3/2}$	$(-3452.7*BF)+326489.1$ $N/m^{3/2}$
		VG	8270 N/m	8270 N/m
		HC	7110 $N/m^{3/2}$	3710 $N/m^{3/2}$
		VO	$(-14.1*TSTT)+1567$ N/m^3	$(-14.1*TSTT)+1567$ N/m^3
b, a		VG	727.1 Ns/m	519.1 Ns/m
		HC	$(-1983.9*PW)+69039.7$ $s/m^{3/2}$	$(-1983.9*PW)+69039.7$ $s/m^{3/2}$
		VO	$(-34177.5*PW)+1285708.3$ s/m	$(-34177.5*PW)+1285708.3$ s/m

Model simulation

Models were simulated in MapleSim (Version 6.4, Maplesoft, Waterloo, ON), a symbolic multibody modeling software package. Initial centre-of-mass displacement of 0.05 m (matching experimental initial conditions) and constant acceleration ($\alpha=9.81$ m/s^2) was assumed for all models. For timepoints where the simulated pelvis was not in contact with the ground, motion was modeled as a state of free fall. Normal force equations for each model are presented in Table 3; these formulae are implemented when the simulated pelvis is in contact with the ground. Centre of mass displacement (δ) is calculated as vertical deflection from the initial contact point.

Table 3 Model normal force formulae

Model	Formula	
MS	$F_N = k_{MS}\delta$	(2)
HZ	$F_N = k_{HZ}\delta^{3/2}$	(3)
VG	$F_N = k_{VG}\delta + b_{VG}\dot{\delta}$	(4)
HC	$F_N = k_{HC}\delta^{3/2} + a_{HC}\delta^{3/2}\dot{\delta}$	(5)
VO	$F_N = k_{VO}V(1 + a_{VO}\dot{\delta})$	(6)

Model evaluation

Models were evaluated based on a within-subjects basis relative to the reference curve (Figure 6) for the criteria outlined in Table 4.

Table 4: Model performance evaluation criteria

| Component	
Err_{max}	The difference between the maximum of the reference curve and the maximum of the simulated curve, as a percent error. Err_{max} provides a gross estimate of the accuracy of each model for predicting load magnitude.
Err_{TTP}	The difference in the Time To Peak interval (TTP; calculated as T_{imp}-T_{max}) between the reference curve and simulated curve, as a percent error. Err_{TTP} provides a gross estimate of the accuracy of each model for predicting loading timing.
Err_{imp}	The difference in impulse (from time point x to y) between the reference curve and simulated curve, as a percent error. Err_{imp} provides a gross estimate of each model for predicting both load magnitude and timing.
Err_{corr}	A simplified corridor evaluation in which the number of simulated data points falling outside the +-2 SD corridor is expressed as a percent error. Err_{corr} provides an estimate of how well each model replicates the size and shape of the loading curve.
Err_{RMSE}	The root-mean-squared error between the reference curve and simulated curve, expressed as a percent of the mean force between T_{imp} and T_{min}. Err_{RMSE} provides an estimate of error in prediction of force magnitude across the loading curve.
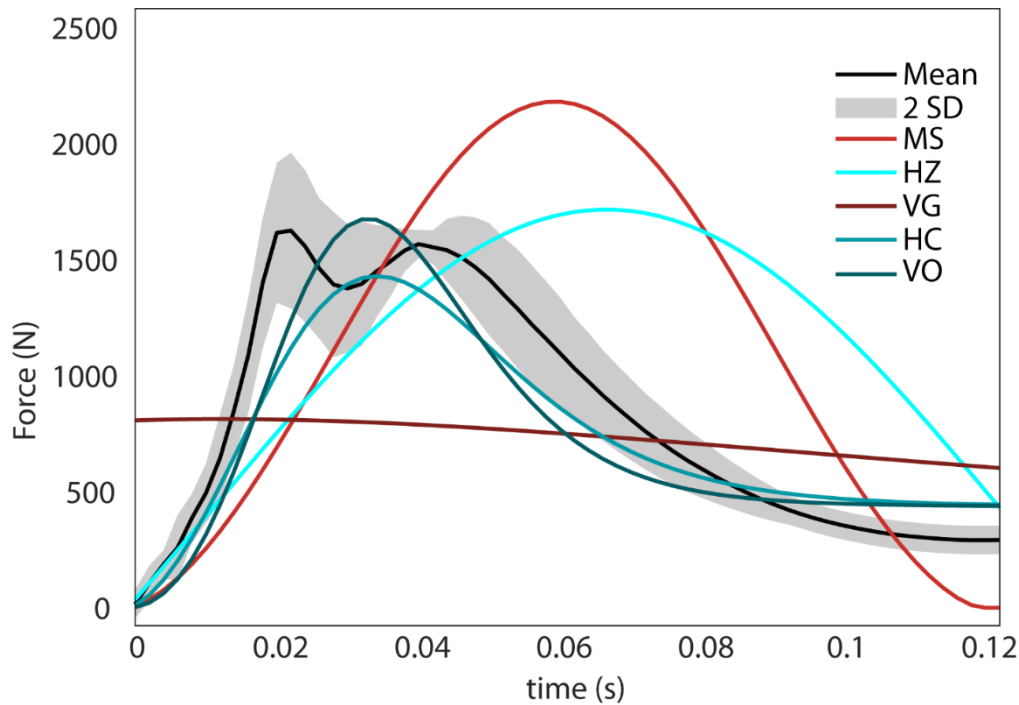
Figure 6: Demonstration of time-varying model performance within the 2 SD (95% CI) corridors. Models were compared against the experimental data (black line, grey band) between the initiation of impact and first minimum following peak force. Models were compared on performance in replicating peak force, time to peak force, impulse, and the percentage of predicted data points within the experimental corridor.

Statistical Analysis

We used a software package to conduct statistical analyses (SPSS version 21, Chicago, USA). Outcomes (Err_{max}, Err_{TTP}, Err_{imp}, Err_{corr} and Err_{RMSE}) were compared across all five models (MS, HZ, VG, HC and VO) via ANOVA, with model type treated as a repeated measure, and an α of 0.05. In addition, two-tailed Pearson correlations were used to examine the relationships between model errors and individual characteristics (*height, mass, BMI, Circ_{hip}, PW, BF, TSTT*) or experimental contact profile (*H0, H1, H2*); a p-value threshold of <0.005 defined 'significant' correlations, adjusted for multiple comparisons; 0.005 > p < 0.05 was defined liberally as a 'trend' to highlight potential relationships or outliers for future analysis.

RESULTS

Performance outcomes differed between models across all criteria (Table 5). Err_{max} differed between all models except for MS and VO; mean errors were large and positive for MS and VO, large and negative for VG, and more moderate (within 12.8%) for HZ and HC (Figure 7a). Time-to-peak errors were similar and moderate for VG and HC, significantly larger and positive for MS and HZ, and larger and negative for VO (Figure 7b). Err_{corr} was substantially lower for HC compared to all other models (Figure 7c). Impulse error was similar and low for VG and VO, 4.5-

6.6% higher for HC, and 26.0-41.8% higher for MS and HZ (Figure 7d). Performance for Err_{RMSE} differed between models, and significantly lower for HC than all other models (Figure 7).

Err_{max} was primarily negatively correlated with indices of body composition: BMI, BF, TSTT (Figure 8a-c). In absolute terms, Err_{max} was lowest for high BF participants for MS, HZ and VO, but lowest for low BF participants for HC. Performance decreased for geometric models as PW increased (HC, VO, Figure 8d) and as contact area increased (VO, Figure 8e). Timing errors followed opposing trends for VG and VO compared to MS, HZ and HC. For VG and VO, Err_{TTP} increased as body size and contact area increased (*Mass, BMI, TSTT, Circ_{hip}, BF* and *H0* for VG, *BMI, PW* for VO, Figure 9a-g). Inverse relationships between Err_{TTP} and body composition (*TSTT, BF,* Figure 9c,e) and contact profile (*H0, H2,* Figure 9g,h) for MS, and HZ were primarily driven by two participants with high Err_{TTP} outcomes. Err_{TTP} for HC followed the directional trends of MS and HZ, but was not strongly influenced by outlying participants, and was lowest for participants with moderate BF and average contact profiles (Figure 9e,g,h). Trends for worse corridor performance with indices of body composition (Figure 10a-c) were weak (all r<0.5) and only apparent for viscoelastic models (VG, HC, VO). Impulse performance was linked to individual characteristics and contact profile for VO (Figure 11), driven by performance for participants at the high extremity of the *BMI, TSTT* and *BF* range. Err_{RMSE} worsened as *BF* decreased for VO (Figure 12a). Err_{RMSE} was also negatively associated with H1 for all geometric models, and H0 and H2 for VO only (Figure 12b-d).

Table 5: Main effects and pairwise comparisons between models for significant model error differences

Model		Err_{max}		Err_{TTP}		Err_{corr}		Err_{imp}		Err_{RMSE}	
F		301.6		54.4		14.1		48.8		18.6	
p		<0.001**		<0.001**		<0.001**		<0.001**		<0.001**	
		MD[1]	p	MD	p	MD	p	MD	p	MD	p
MS	HZ	31.8	<0.001**	-20.4	<0.001**	-0.9	0.538	-9.2	<0.001**	15.1	<0.001**
	VG	92.9	<0.001**	65.7	<0.001**	2.4	0.393	-41.3	<0.001**	32.7	<0.001**
	VO	6.9	0.095	92.8	<0.001**	-3.7	0.208	-39.1	<0.001**	49.1	<0.001**
	HC	50.1	<0.001**	67.3	<0.001**	-14.0	<0.001**	-34.5	<0.001**	15.7	0.018*
HZ	MS	-.1.8	<0.001**	20.4	<0.001**	0.9	0.538	9.2	<0.001**	-15.1	<0.001**
	VG	61.1	<0.001**	86.1	<0.001**	3.4	0.144	-32.1	<0.001**	17.6	0.001**
	VO	-24.9	<0.001**	113.2	<0.001**	-2.8	0.266	-29.8	<0.001**	34.0	<0.001**
	HC	19.2	<0.001**	87.7	<0.001**	-13.0	<0.001**	-25.3	<0.001**	0.6	0.936
VG	MS	-92.9	<0.001**	-65.7	<0.001**	-2.4	0.393	41.3	<0.001**	-32.7	<0.001**
	HZ	-61.1	<0.001**	-86.1	<0.001**	-34.0	0.144	32.1	<0.001**	-17.6	0.001**
	VO	-86.0	<0.001**	27.1	0.002**	-6.1	<0.001**	2.2	0.560	16.4	0.001**
	HC	-42.8	<0.001**	1.6	0.874	-16.4	<0.001**	6.8	0.004**	-17.0	0.051
VO	MS	-6.9	0.095	-92.8	<0.001**	3.7	0.208	39.1	<0.001**	-49.1	<0.001**
	HZ	24.8	<0.001**	-113.2	<0.001**	2.8	0.266	29.8	<0.001**	34.0	<0.001**
	VG	86.0	<0.001**	-27.1	0.002**	6.1	<0.001**	-2.2	0.560	-16.4	<0.001
	HC	43.2	<0.001**	-25.5	<0.001**	-10.3	<0.001**	4.5	0.243	-33.4	<0.001**
HC	MS	-50.1	<0.001**	-67.3	<0.001**	14.0	<0.001**	34.5	<0.001**	-15.7	0.018*
	HZ	-18.3	<0.001**	-87.7	<0.001**	13.0	<0.001**	25.3	<0.001**	-0.6	0.936
	VG	42.8	<0.001**	-1.6	0.874	16.4	<0.001**	-6.8	0.004**	17.0	0.051
	VO	-43.2	<0.001**	25.5	<0.001**	10.3	<0.001**	-4.5	0.243	33.4	<0.001**

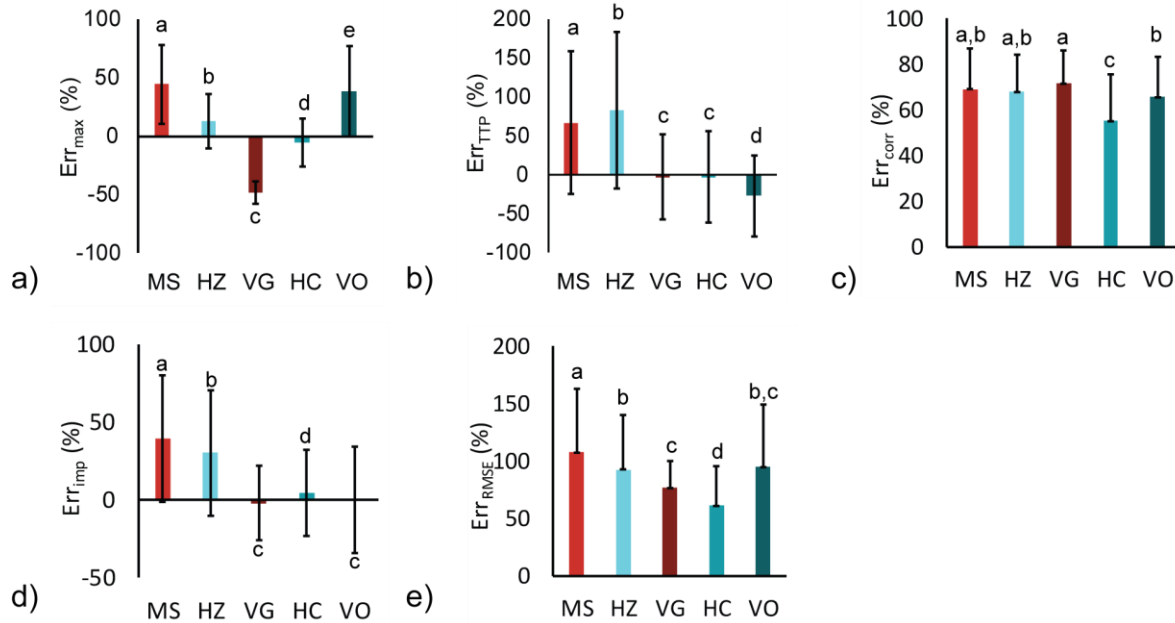*Significant comparison at p<0.05 ** Significant comparison at p<0.01*

Figure 7: Model performance across criteria. Model performance varied, with HC consistently performing within the most accurate group across criteria. A geometry-damping interaction revealed a directional effect of damping and magnitude effect of geometry on Err_{max} (a), while the timing improvement introduced by damping components in Err_{TTP} (b) carried through to better performance in Err_{corr} (c), Err_{imp} (d), and Err_{RMSE} (e). Homogeneous subsets, based on pairwise comparisons, are indicated with letters (a, b . . .).
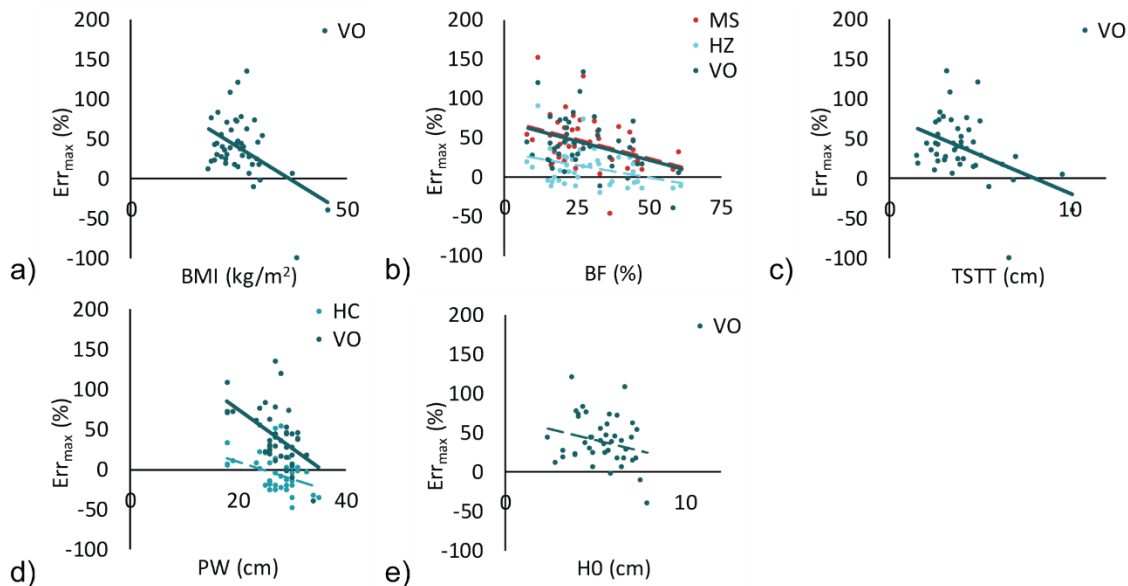

Figure 8: Trends in Err_{max} magnitude were driven primarily by body composition (a,b,c) for MS, HZ and VO. Most consistently, BF produced more accurate peak force predictions at high levels of body fat for MS, HZ and VO. Additionally, Err_{max} performance for HC and VO, both geometric models, decreased as PW increased (d). There was also a trend for decreased Err_{max} at higher contact area (H0) for VO (e). Significant relationships are indicated with solid lines; trends are indicated with dashed lines.
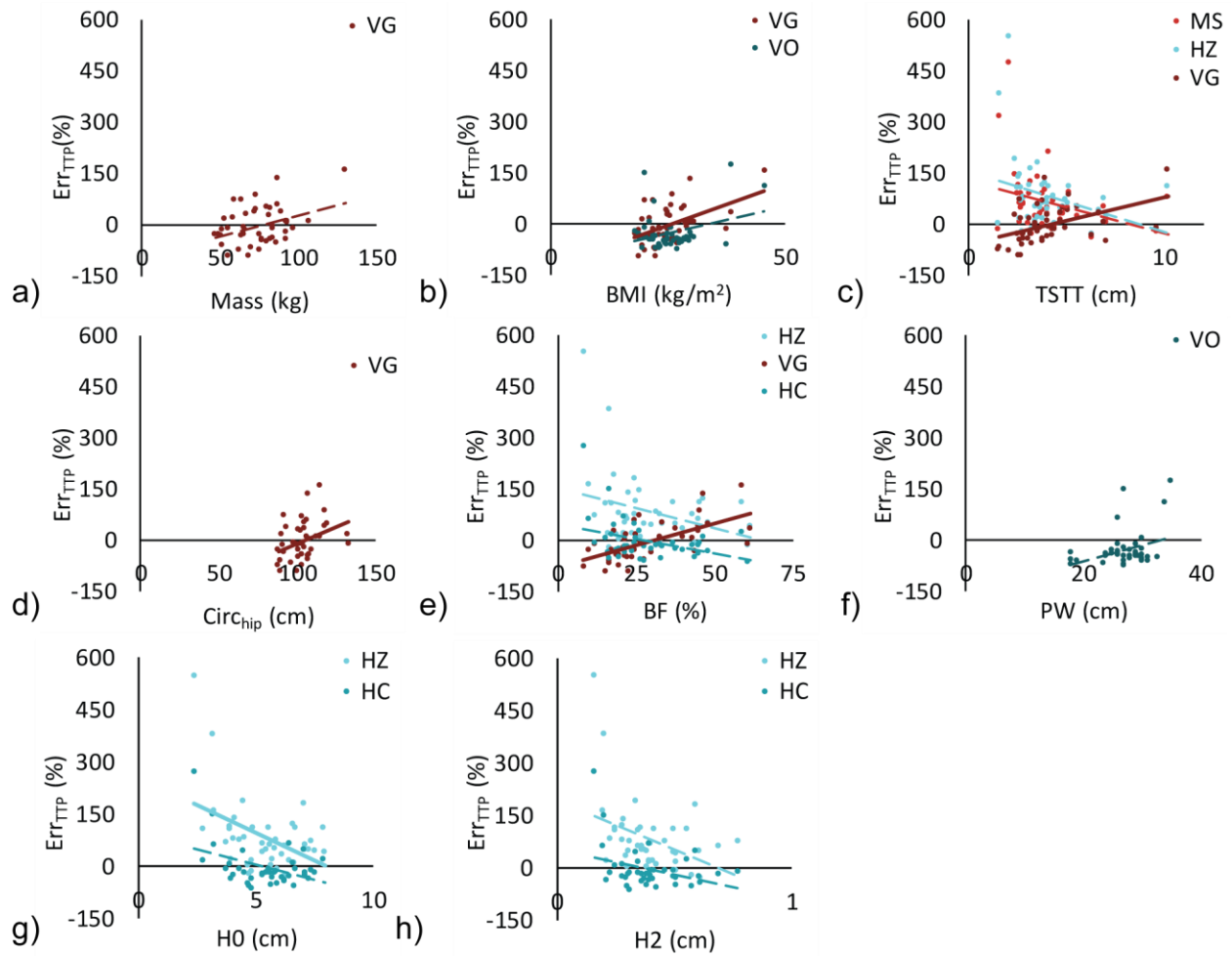
Figure 9: Along with a relationship trend between *Err*$_{TTP}$ and *Mass* (a), *Err*$_{TTP}$ was significantly positively associated with *BMI, TSTT, Circ*$_{hip}$ and *BF* for VG (b, c, d, e). A trend for increased *Err*$_{TTP}$ linked to higher *BMI* and *PW* was observed for VO. A trend for decreased *Err*$_{TTP}$ with increased *TSTT* was observed for MS and HZ (c), and with increasing *BF* for HZ and HC (e). A significant negative relationship between H0 (mean contact area radius) and *Err*$_{TTP}$ was observed for HZ and HC. A negative trend between H2 (ellipticality) and *Err*$_{TTP}$ was found for HZ and HC (h). Significant relationships are indicated with solid lines; trends are indicated with dashed lines.
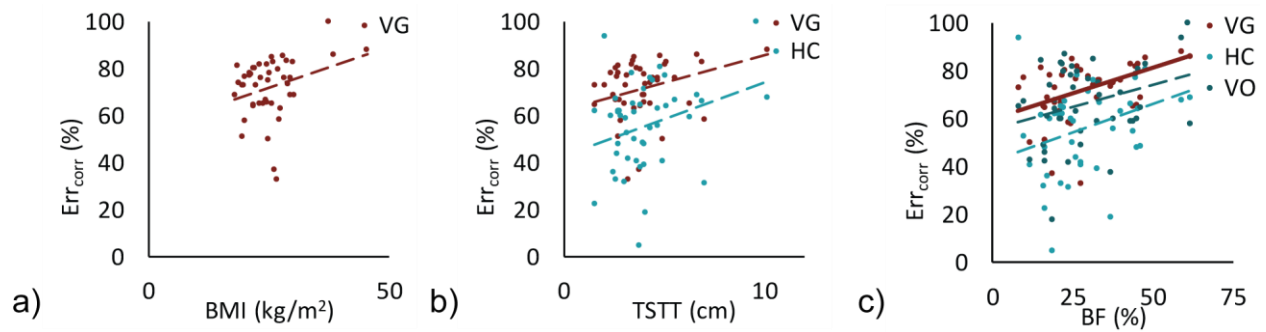
14

Figure 10: Corridor error trended positively (i.e. worse performance) with increased *BMI* for VG (a), increased *TSTT* for VG and HC (b). Trends between worse Err_{corr} performance and increased *BF* for VO and HC, and a significant relationship between Err_{corr} and *BF* were found for VG (c). There were no significant correlations between Err_{corr} and overall body size, skeletal dimensions or pelvis-ground contact metrics. Significant relationships are indicated with solid lines; trends are indicated with dashed lines.
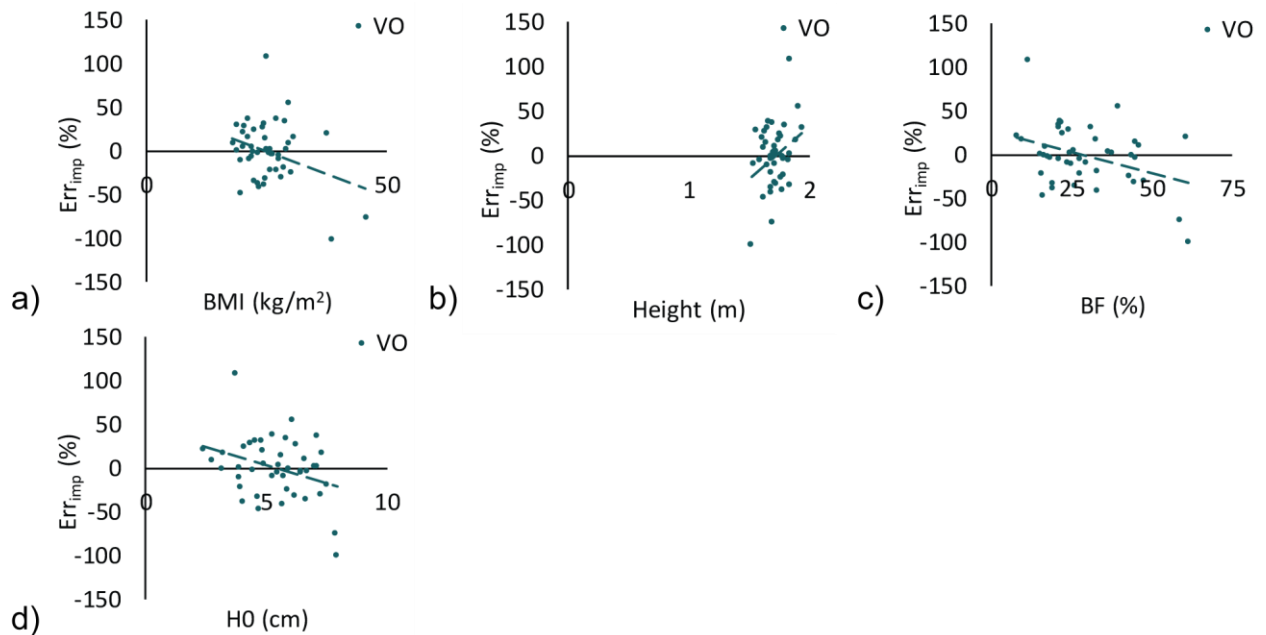

Figure 11: Trends were observed only for VO: a generally negative relationship between Err_{imp} performance, and *BMI* (a), *Height* (b), *BF* (c) and *H0* (d). Significant relationships are indicated with solid lines; trends are indicated with dashed lines.
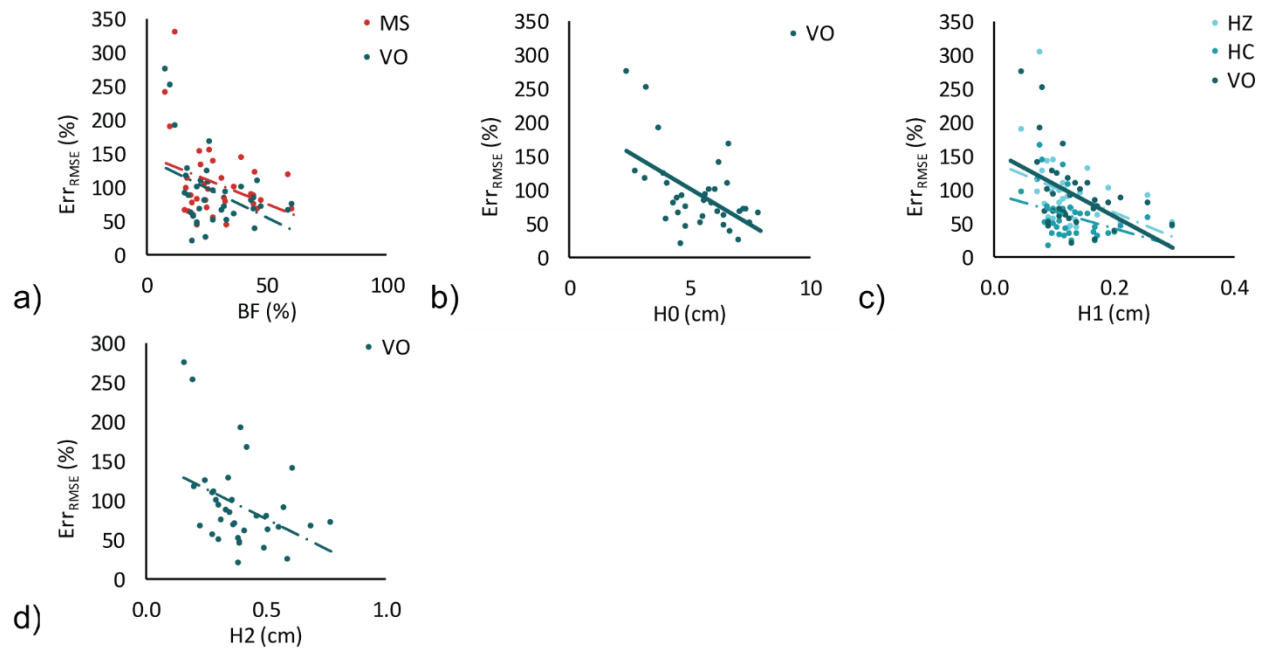
Figure 12: A negative trend between Err_{RMSE} and BMI was found for VO and MS (a). Err_{RMSE} was also negatively linked to contact area (significant for VO, b), H1 (significant for VO, trend for HZ and HC, c) and H2 (trend for VOb). There were no links between Err_{RMSE} and skeletal dimensions (*height* or *PW*). Significant relationships are indicated with solid lines; trends are indicated with dashed lines.

Table 6 Correlation between peak model performance outcomes and individual characteristics, r (p)

		Individual Characteristics							Experimental Contact Profile		
		Height	*Mass*	*BMI*	*TSTT*	*PW*	*Circ$_{hip}$*	*BF*	H0	H1	H2
Err_{max}	MS	0.213 (0.155)	-0.058 (0.702)	-0.200 (0.182)	-0.125 (0.409)	-0.028 (0.854)	-0.164 (0.281)	-0.384* (0.010)	-0.179 (0.245)	NA	NA
	HZ	0.160 (0.287)	-0.066 (0.664)	-0.184 (0.220)	-0.111 (0.464)	-0.051 (0.738)	-0.171 (0.260)	-0.359* (0.017)	-0.201 (0.192)	NA	NA
	VG	0.135 (0.371)	0.010 (0.947)	-0.078 (0.608)	-0.022 (0.887)	-0.037 (0.808)	-0.143 (0.347)	-0.247 (0.106)	-0.199 (0.194)	-0.142 (0.356)	0.098 (0.527)
	HC	0.121 (0.423)	-0.107 (0.481)	-0.206 (0.170)	-0.140 (0.355)	-0.386* (0.008)	-0.101 (0.511)	-0.250 (0.102)	-0.213 (0.166)	-0.211 (0.169)	0.031 (0.843)
	VO	0.286 (0.054)	-0.242 (0.106)	-0.464** (0.001)	-0.443** (0.002)	-0.587** (<0.001)	-0.097 (0.526)	-0.488** (0.001)	-0.350* (0.020)	-0.238 (0.120)	-0.095 (0.541)
Err_{TTP}	MS	0.149 (0.327)	-0.108 (0.479)	-0.179 (0.240)	-0.311* (0.038)	-0.137 (0.369)	-0.217 (0.157)	-0.283 (0.066)	-0.437** (0.003)	NA	NA
	HZ	0.173 (0.251)	-0.121 (0.423)	-0.206 (0.169)	-0.322* (0.029)	-0.128 (0.396)	-0.223 (0.141)	-0.311* (0.040)	-0.451** (0.002)	NA	NA
	VG	-0.145 (0.335)	0.371* (0.011)	0.491** (0.001)	0.454** (0.002)	0.276 (0.064)	0.368* (0.013)	0.635** (<0.001)	0.598** (<0.001)	0.174 (0.259)	0.192 (0.211)
	HC	0.223 (0.150)	-0.055 (0.727)	-0.166 (0.287)	-0.298 (0.052)	0.067 (0.671)	-0.253 (0.106)	-0.376* (0.014)	-0.418* (0.007)	-0.045 (0.779)	-0.341* (0.029)
	VO	-0.112 (0.458)	0.187 (0.213)	0.321* (0.029)	0.165 (0.274)	0.328* (0.026)	-0.208 (0.171)	0.136 (0.378)	-0.040 (0.794)	0.090 (0.562)	-0.93 (0.547)

* Trend at p<0.05 ** Significant comparison at p<0.005

Table 7 Correlation between time-varying model performance outcomes and individual characteristics, r (p)

		Individual Characteristics							Experimental Contact Profile		
		Height	*Mass*	*BMI*	*TSTT*	*PW*	*Circ_{hip}*	*BF*	*H0*	*H1*	*H2*
Err_{imp}	MS	-0.223 (0.137)	0.031 (0.837)	0.167 (0.267)	0.116 (0.443)	0.000 (0.998)	0.025 (0.870)	0.218 (0.156)	0.147 (0.340)	NA	NA
	HZ	-0.157 (0.299)	0.113 (0.454)	0.227 (0.129)	0.140 (0.352)	0.042 (0.784)	0.051 (0.738)	0.246 (0.107)	0.176 (0.254)	NA	NA
	VG	-0.166 (0.269)	0.130 (0.390)	0.242 (0.104)	0.151 (0.317)	0.079 (0.602)	0.094 (0.541)	0.258 (0.091)	0.249 (0.103)	0.129 (0.403)	-0.012 (0.939)
	HC	-0.153 (0.311)	-0.001 (0.997)	0.096 (0.527)	0.039 (0.798)	0.019 (0.901)	0.008 (0.961)	0.098 (0.525)	0.158 (0.306)	0.263 (0.085)	-0.049 (0.751)
	VO	-0.310* (0.036)	0.112 (0.458)	-0.324* (0.028)	0.219 (0.144)	0.013 (0.992)	0.038 (0.803)	-0.378* (0.012)	-0.342* (0.023)	0.239 (0.117)	0.077 (0.618)
Err_{corr}	MS	-0.001 (0.993)	-0.030 (0.841)	-0.020 (0.895)	-0.021 (0.888)	0.042 (0.781)	-0.124 (0.416)	0.055 (0.724)	0.074 (0.632)	NA	NA
	HZ	0.083 (0.585)	-0.041 (0.787)	-0.087 (0.565)	-0.058 (0.701)	0.103 (0.495)	-0.124 (0.416)	-0.072 (0.641)	0.121 (0.432)	NA	NA
	VG	0.194 (0.198)	-0.150 (0.320)	-0.297* (0.045)	-0.335 (0.023)	0.054 (0.724)	-0.267 (0.076)	-0.447** (0.002)	-0.250 (0.101)	-0.022 (0.890)	0.091 (0.555)
	HC	0.252 (0.091)	0.003 (0.983)	-0.148 (0.326)	-0.300* (0.043)	0.181 (0.229)	-0.162 (0.289)	-0.343* (0.023)	-0.103 (0.505)	-0.012 (0.938)	0.148 (0.339)
	VO	0.185 (0.219)	-0.024 (0.875)	-.127 (0.400)	-0.219 (0.145)	0.250 (0.094)	-0.227 (0.133)	-0.305* (0.044)	-0.114 (0.462)	0.001 (0.997)	0.079 (0.611)
Err_{RMSE}	MS	0.242 (0.149)	0.004 (0.983)	-0.113 (0.504)	0.007 (0.967)	0.004 (0.981)	-0.191 (0.264)	-0.339* (0.043)	0.003 (0.989)	NA	NA
	HZ	0.267 (0.110)	0.085 (0.616)	-0.039 (0.817)	0.036 (0.834)	0.046 (0.789)	-0.155 (0.365)	-0.279 (0.099)	0.111 (0.566)	NA	NA
	VG	0.118 (0.487)	0.054 (0.753)	0.000 (0.999)	0.141 (0.404)	-.005 (0.977)	-0.022 (0.897)	-0.105 (0.541)	-0.313 (0.067)	-0.398* (0.018)	-0.072 (0.680)
	HC	0.172 (0.308)	-0.012 (0.944)	-0.089 (0.602)	0.042 (0.806)	0.006 (0.971)	-0.135 (0.433)	-0.295 (0.081)	-0.208 (0.230)	-0.382* (0.024)	-0.161 (0.355)
	VO	0.106 (0.534)	-0.231 (0.170)	-0.302 (0.069)	-0.160 (0.343)	-0.036 (0.831)	-0.212 (0.215)	-0.420 (0.011)	-0.543** (0.001)	-0.451** (0.004)	-0.387* (0.022)

* Trend at $p<0.05$ ** Significant comparison at $p<0.005$

DISCUSSION

We aimed to determine how increased model complexity, through inclusion of damping and geometric components, improved replication of the impact phase of a fall to the hip in a controlled, experimental setting. Geometry strongly affected peak force prediction, however, damping had a stronger effect on timing, which carried through to better replication of the impact impulse, as well as performance in the corridor and RMSE criteria. The Hunt-Crossley model performed consistently well across all five criteria. Regarding the second goal, we tied errors in current model iterations to individual and characteristics and contact profile, which can be linked to theoretical limitations or actionable changes for each model.

Damping affected Err_{TTP} substantially, highlighting the importance of the viscoelasticity of the pelvis system on loading behavior. The loading period of a pelvis release is less than 0.1s (Laing, 2010; Levine, 2013), but the stress-relaxation period of hip-region soft tissues is substantially longer (Gefen, 2007; Palevski, 2006). Soft tissues are loaded more rapidly than force can be dissipated, resulting in greater initial stress generation (i.e. higher peak forces and lower system deformation). VG provided a 64.0% improvement over MS, while HC provided an 86.1% improvement over HZ. Improvements carried forward in stronger prediction of the impact impulse and replication of the experimental corridor. However, variance in Err_{TTP} for VG (Figure 7b), along with the poor characterization of VG (Figure 6) demonstrates that success of damping characterization differs between subjects.

Errors for Err_{TTP}, Err_{corr} and Err_{imp} related to body composition and contact profile, highlighting the three-dimensional viscoelastic interaction over a simpler models. For VG, time-to-peak was underestimated for participants with low body fat and contact area, and overestimated for participants with high BF and $H0$. While the damping component of VG improves Err_{TTP} over MS, sensitivity to body composition and contact profile indicates that SDF assumptions have been violated, specifically, 1) contact between the pelvis and ground has a more-than-minimal effect on the loading response, and, 2) the viscous response is not linearly related to vertical pelvis velocity. These assumptions were addressed via HC and VO models, for which Err_{TTP}, Err_{corr} and Err_{imp} may be improved in future models through incorporation of BF into the damping parameter predictive equation (Table 2). This may lead to more accurate recreation of non-linear loading profiles and the energy-dissipative effect of soft tissues.

Conversely, geometry, not damping, influenced Err_{max} via load distribution. However, performance improvement was minimal across criteria for the most geometrically-complex model, VO. Comparatively, HC performed within the best subset for four out of five criteria, substantially better than MS for all criteria. This may arise from error in characterizing additional parameters for VO (i.e. pelvis sphere diameter) or mismatch between pelvis geometry during the impact phase and sphere-on-plane representation. VO was sensitive to contact profile components in three out of five error criteria, particularly at extreme values of $H0$, $H1$ and $H2$. Sensitivity of VO to deviance from the expected contact profile may warrant different interference geometry (e.g. cylinder-on-plane rather than sphere-on-plane).

Further, force is substantially localized within the pelvis contact profile (Choi, 2010; Laing, 2010) which is likely better represented by HC than VO (Figure 13). VO performance was particularly poor for participants at the upper and lower extremes of *BF, TSTT* and H0-H2. Shourijeh (2015) developed a hyper-volumetric foot model (volumetric model with hyperelastic, non-linear foundation), to account for large deformation of soft tissue, which is more deformable than standard engineering materials. While this may be a fruitful approach for a lateral hip impact scenario, it is unclear whether the improvement would be worth additional cost of parameter development and computation, considering the positive performance of the simpler Hunt-Crossley model.

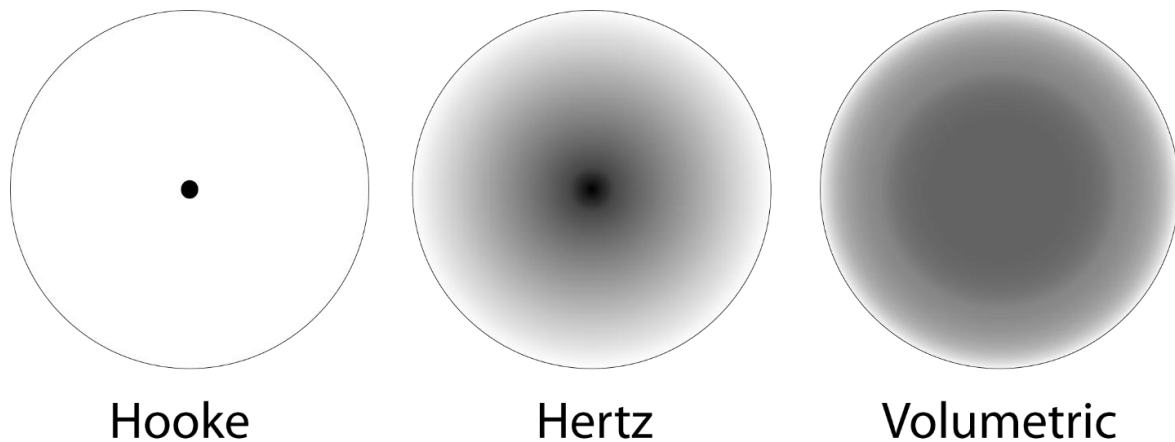## Hooke   Hertz   Volumetric

Figure 13: For models based on Hookean theory (MS, VG), pressure is assumed to be applied at a single central point. For models based on Hertz theory (HZ, HC), pressure is concentrated at a single central point. In the volumetric model, pressure is distributed away from the central contact point, dependent on the depth of interaction between the sphere and plane.

It is valuable to carry forward our results to consider load application in finite element models and other paradigms for internal load modeling of the pelvis-femur system. The models developed here can be used to generate a subject-specific spatial matrix of force inputs for detailed finite element models (e.g. Majumder, 2004, 2013; Ferdous, 2015; Sarvi, 2015). Partitioning stress along the modeled components in a Hertzian-based pressure distribution may improve biofidelity over a point load at the greater trochanter. This approach can improve understanding of how individual body composition affects localized stress within anatomical components.

From a factor-of-risk perspective, accurate estimation of impact force during falls to the hip is critical for predicting hip fracture. We were able to predict applied loads within a mean (SD) of 5.4 (20.7)% for HC; however, the model, in its current implementation, is limited to a directly lateral hip impact, with an impact configuration similar to the pelvis release body configuration. Bouxsein et al. (2007) used a mass-spring model to estimate TSTT-attenuated peak force for hip fracture cases and older adult faller controls, finding this method of distinguishing fracture cases from controls was effective for women, but not men (Nielson, 2009). Using a three-link (torso,

thigh, shank) whole-body dynamics model with a Voigt impact model, Sarvi (2015) developed an individual-specific model of falls from standing height, finding a substantial effect of TSTT and obesity or underweight on fall force estimates. Upon validating the model experimentally (Sarvi, 2014), peak force estimation error was similar VG in this study; however, our results show that loading-response replication may be improved by substituting VG with a Hunt-Crossley formulation. A stronger contact model would improve performance of multi-level modeling of falls.

Our findings enhance the body of evidence supporting simplified-geometry-based multi-segment biomechanical modeling approaches. Hertzian models have previously been successfully used to simulate deep tissue injuries resulting from prolonged sitting (Gefen, 2007), as well as cartilaginous joints under static conditions (Eberhardt, 1991; Hirokawa, 1991). Queen (2003) used a Hertzian model to simulate soccer heading, reporting that soccer ball dimension affected heading kinematics moreso than inflation pressure (i.e. stiffness), but did not discuss the potential of a viscoelastic component. Lintern (2015) successfully implemented a Hunt-Crossley model to simulate brain trauma during an infant shaking paradigm. Shourijeh (2015) and Lopes (2016) found substantial improvement in ground reaction force prediction using a volumetric model to simulate foot contact during level gait compared to a point-contact model. Together, these successes support development of a dynamic multibody systems approach for rapid estimation of loading magnitude, distribution and injury risk across multiple body regions.

Limitations of the current work support development of future modeling strategies. First, though we included overall corridor performance in this study, we did not identify regions of poor concordance between the experimental and simulated data. Qualitatively, an inflection point (Figure 14) in the experimental data was a region of poor concordance. This feature may signify a change in the dominant anatomical or system components (e.g. a soft-tissue-dominated phase followed by a skeletal-tissue-dominated phase). Accordingly, a multiphase model may better represent this behavior. Second, we simulated normal force during a directly lateral impact to the pelvis. Further development should include more complex impact configurations; this highlights VO over simpler models. Resistance to tangential rolling, and tangential friction between the pelvis and floor can be modeled within the Volumetric framework, which may be important in simulating more complex impact configurations. Third, we characterized and validated our model parameters at low (but clinically-relevant (Choi, 2015)) impact velocities. The stiffness and damping behaviors of the pelvis may differ at higher impact velocities. Validation at higher impact velocities, and implementation of a factor-of-risk based epidemiological model would be of value to determine whether performance of HC extends to predicting injurious falling scenarios.
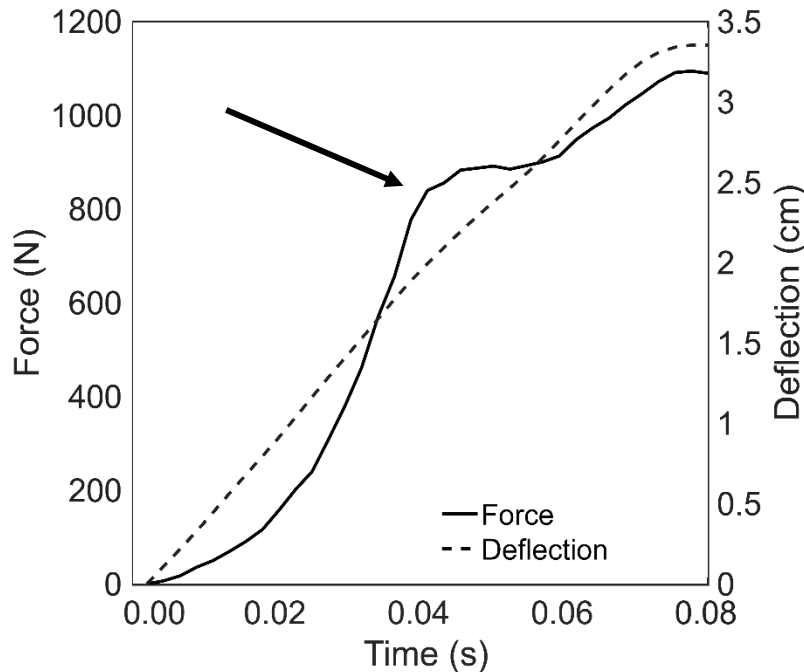
Figure 14: Nonlinearity in the force and deflection data during the initial impact phase. During the initial phase of the impact, the loading response (solid line) is typically non-linear. Loading responses typically include a "shoulder region" (black arrow) which was not captured by any of the models in this study. In contrast, the deflection response (dashed line) is primarily linear.

CONCLUSIONS

We compared contact models with geometric and damping components. Geometric components had a stronger effect peak force prediction, while damping components had a stronger effect on timing characteristics. Both factors interacted to influence impulse and corridor rating, which are dependent on both timing and magnitude of loading. The Hunt-Crossley model performed the best within this study, and is relatively simple and efficient to implement—therefore, this may be the most appropriate model for simulation of prediction of impact dynamics in the lateral fall configuration we investigated. Model errors were sensitive to body composition and contact profile, tied to theoretical limitations or actionable changes for each model.

ACKNOWLEDGEMENTS

REFERENCES

BOUXSEIN, M., SZULC, P., MUNOZ, F., THRALL, E., SORNAY-RENDU, E., & DELMAS, P. (2007). Contribution of Trochanteric Soft Tissues to Fall Force Estimates, the Factor of Risk, and Prediction of Hip Fracture Risk*. Journal of Bone and Mineral Research, 22(6), 825-831.

CHOI, W. J., HOFFER, J. A., & ROBINOVITCH, S. N. (2010). Effect of hip protectors, falling angle and body mass index on pressure distribution over the hip during simulated falls. Clinical Biomechanics, 25(1), 63-69.

EBERHARDT, A., LEWIS, J., & KEER, L. (1991). Normal contact of elastic spheres with two elastic layers as a model of joint articulation. J Biomech Eng, 113(4), 410-417.

EHRLICH, R., & WEINBERG, B. (1970). An exact method for characterization of grain shape. Journal of Sedimentary Research, 40(1), 205-212.

FERDOUS, Z., & LUO, Y. (2015). Study of hip fracture risk by DXA-based patient-specific finite element model. Bio-medical materials and engineering, 25(2), 213-220.

FREGLY, B. J., BEI, Y., & SYLVESTER, M. E. (2003). Experimental evaluation of an elastic foundation model to predict contact pressures in knee replacements. Journal of biomechanics, 36(11), 1659-1668.

GEFEN, A. (2007). Risk factors for a pressure-related deep tissue injury: a theoretical model. Medical & biological engineering & computing, 45(6), 563-573.

GEFEN, A., & HABERMAN, E. (2007). Viscoelastic properties of ovine adipose tissue covering the gluteus muscles. Journal of biomechanical engineering, 129(6), 924-930.

HIROKAWA, S. (1991). Three-dimensional mathematical model analysis of the patellofemoral joint. Journal of biomechanics, 24(8), 659-671.

HUNT, K., & CROSSLEY, F. (1975). Coefficient of restitution interpreted as damping in vibroimpact. Journal of Applied Mechanics, Transactions ASME, 42 (2), 440-445.

JACKSON, A. S., & POLLOCK, M. L. (1978). Generalized equations for predicting body density of men. British journal of nutrition, 40(03), 497-504.

JACKSON, A. S., POLLOCK, M. L., & WARD, A. N. N. (1979). Generalized equations for predicting body density of women. Medicine and science in sports and exercise, 12(3), 175-181.

LAING, A. C., & ROBINOVITCH, S. N. (2010). Characterizing the effective stiffness of the pelvis during sideways falls on the hip. Journal of biomechanics, 43(10), 1898-1904.

LAING, A. C., TOOTOONCHI, I., HULME, P. A., & ROBINOVITCH, S. N. (2006). Effect of compliant flooring on impact force during falls on the hip. Journal of Orthopaedic Research, 24(7), 1405-1411.

LEVINE, I. C. (2017a). The effects of body composition and body configuration on impact dynamics during lateral falls: insights from in-vivo, in-vitro, and in-silico approaches. UWSpace: http://hdl.handle.net/10012/12584.

LEVINE, I. C., BHAN, S., & LAING, A. C. (2013). The effects of body mass index and sex on impact force and effective pelvic stiffness during simulated lateral falls. Clinical Biomechanics, 28(9), 1026-1033.

LEVINE, I. C., & LAING, A. C. (2017, May 21-23, 2017b). Peak pressure and contact profile: links with individual characteristics and falling configuration. Paper presented at the 13th Annual Injury Biomechanics Symposium, Columbus, Ohio.

LINTERN, T., GAMAGE, N. P., BLOOMFIELD, F., KELLY, P., FINCH, M., TABERNER, A., . . . NIELSEN, P. (2015). Head kinematics during shaking associated with abusive head trauma. Journal of biomechanics, 48(12), 3123-3127.

LOPES, D., NEPTUNE, R., AMBRÓSIO, J., & SILVA, M. (2016). A superellipsoid-plane model for simulating foot-ground contact during human gait. Computer methods in biomechanics and biomedical engineering, 19(9), 954-963.

MAJUMDER, S., ROYCHOWDHURY, A., & PAL, S. (2004). Dynamic response of the pelvis under side impact load–a three-dimensional finite element approach. International Journal of Crashworthiness, 9(1), 89-103.

MAJUMDER, S., ROYCHOWDHURY, A., & PAL, S. (2013). Hip fracture and anthropometric variations: Dominance among trochanteric soft tissue thickness, body height and body weight during sideways fall. Clinical Biomechanics, 28(9), 1034-1040.

NIELSON, C. M., BOUXSEIN, M. L., FREITAS, S. S., ENSRUD, K. E., & ORWOLL, E. S. (2009). Trochanteric soft tissue thickness and hip fracture in older men. Journal of Clinical Endocrinology & Metabolism, 94(2), 491-496.

PALEVSKI, A., GLAICH, I., PORTNOY, S., LINDER-GANZ, E., & GEFEN, A. (2006). Stress relaxation of porcine gluteus muscle subjected to sudden transverse deformation as related to pressure sore modeling. Journal of biomechanical engineering, 128(5), 782-787.

QUEEN, R. M., WEINHOLD, P. S., KIRKENDALL, D. T., & YU, B. (2003). Theoretical study of the effect of ball properties on impact force in soccer heading. Medicine & Science in Sports & Exercise, 35(12), 2069-2076.

ROBINOVITCH, S., HAYES, W., & MCMAHON, T. (1991). Prediction of femoral impact forces in falls on the hip. Journal of biomechanical engineering, 113(4), 366-374.

ROBINOVITCH, S., HAYES, W., & MCMAHON, T. (1997a). Distribution of contact force during impact to the hip. Annals of biomedical engineering, 25(3), 499-508.

ROBINOVITCH, S., HAYES, W., & MCMAHON, T. (1997b). Predicting the impact response of a nonlinear single-degree-of-freedom shock-absorbing system from the measured step response. Journal of biomechanical engineering, 119(3), 221-227.

ROBINOVITCH, S. N., EVANS, S. L., MINNS, J., LAING, A. C., KANNUS, P., CRIPTON, P. A., . . . LAURITZEN, J. B. (2009). Hip Protectors: Recommendations for Biomechanical Testing – an International Consensus Statement (part I). Osteo Int, 20(12), 1977-1988.

SARVI, M. N., & LUO, Y. (2015). A Two-Level Subject-Specific Biomechanical Model for Improving Prediction of Hip Fracture Risk. Clinical Biomechanics.30 (8), 881-887.

SARVI, M. N., LUO, Y., SUN, P., & OUYANG, J. (2014). Experimental validation of subject-specific dynamics model for predicting impact force in sideways fall. Journal of Biomedical Science and Engineering, 7(07), 405-418.

SHOURIJEH, M. S., & MCPHEE, J. (2015). Foot-ground contact modeling within human gait simulations: from Kelvin-Voigt to hyper-volumetric models. Multibody System Dynamics, 35(4), 393-407.

STINCHCOMBE, A., KURAN, N., & POWELL, S. (2014). Seniors' falls in Canada: Second report: Key highlights. Chronic Diseases and Injuries in Canada, 34(2-3), 171-174.